Contents lists available at ScienceDirect

International Journal of Non-Linear Mechanics

The nature of the normal form map for soft impacting systems

Yue Ma[a], James Ing[b], Soumitro Banerjee[c,*], Marian Wiercigroch[b], Ekaterina Pavlovskaia[b]

[a]Spatio-Temporal Order Project, ICORP, JST, Department of Physics, Graduate School of Science, Kyoto University, Japan
[b]Centre for Applied Dynamics Research, School of Engineering, University of Aberdeen, UK
[c]Centre for Theoretical Studies and Department of Electrical Engineering, Indian Institute of Technology, Kharagpur, India

ABSTRACT

Soft impacting mechanical systems—where the impacting surface is cushioned with a spring–damper support—are common in engineering. Mathematically such systems come under the description of *switching dynamical systems*, where the dynamics toggle between two (or more) sets of differential equations, determined by *switching conditions*. It has been shown that the Poincaré map of such a system would have a power of 1/2 (the so-called square-root singularity) if the vector fields at the two sides of the switching manifold differ, and a power of 3/2 if they are the same. These results were obtained by concentrating on the leading order terms in a Taylor expansion of the zero-time discontinuity map, and are true in the immediate neighbourhood of a grazing orbit. In this paper we investigate how the character of the two-dimensional map changes over a large parameter range as the system is driven from a non-impacting orbit to an impacting orbit. This study leads to vital conclusions regarding the character of the normal form of the map not only in the immediate vicinity of the grazing orbit, but also away from it, as dependent on the system parameters. We obtain these characteristics by experiment and by simulation.

© 2008 Elsevier Ltd. All rights reserved.

1. Introduction

There are a large number of mechanical systems of practical interest in which impacting motion occurs between elements. That is why the fundamental nature of the impacting motion, and the resulting dynamical phenomena have been a matter of great interest. Recent years have seen considerable interest in such non-smooth systems, in particular applied to single degree-of-freedom piecewise oscillators subject to periodic external forcing. The area initiated decades ago by Kobrynskii [1], Feigin [2], and Filippov [3,4] has recently grown extensively, with many theoretical studies addressing specific problems. The investigations by Shaw and Homes [5], Nordmark [6], Peterka and Vacik [7], Lenci and Rega [8], Hogan [9], Blazejczyk-Okolewska and Kapitaniak [10], Budd and Dux [11], and Chin et al. [12], can serve as examples. Generalization of systems with discontinuities has been proposed by Wiercigroch [13,14]. Although some experimental studies on piecewise or impacting systems have been carried out (see, for example, [15–18]), there is a large disproportion between the quantity and quality of theoretical and experimental results. Therefore, in order to understand the laws of motion of non-smooth systems it is essential to gather convincing experimental data, which can be used for the estimation of system characteristics, and for verification of adopted models.

The above studies have provided evidence that such systems can give rise to very rich dynamics, including high-periodic behaviour, quasiperiodicity, and chaos. Most interesting among these phenomena are those which are caused by the transition from non-impacting state to an impacting state, with the critical *grazing* condition acting as the boundary between two different types of dynamical behaviours. The dynamical transitions or bifurcations caused by grazing have therefore been the focus of research in this area.

It is convenient to analyse such phenomena through discrete-time representation. Moreover, if one is interested only in the nature of bifurcations caused by grazing, it is convenient to consider the map in the neighbourhood of the grazing condition. Nordmark [6] considered this representation for an impact oscillator with hard impact against a rigid wall, and showed that the map must have the functional form

$$
\begin{aligned}
x_{n+1} &= ax_n + y_n + \rho \\
y_{n+1} &= -bx_n
\end{aligned}
\quad\Biggr\}
\quad \text{if } x_n \leqslant 0,
$$

$$
\begin{aligned}
x_{n+1} &= -c\sqrt{x_n} + y_n + \rho \\
y_{n+1} &= -dx_n
\end{aligned}
\quad\Biggr\}
\quad \text{if } x_n \geqslant 0.
$$

(1)

The square-root term causes the derivative to approach infinity as $x_n \to 0^+$, resulting in locally infinite stretching of the phase space, called the *square-root singularity*. Subsequently, many researchers

* Corresponding author. Tel.: +91 9434029433; fax: +91 322282262.
E-mail addresses: soumitro@ee.iitkgp.ernet.in, soumitro.banerjee@gmail.com (S. Banerjee).

[12,19] investigated maps of this form to understand the dynamics of the impact oscillator.

Stick-slip oscillation caused by dry friction has also caught significant research attention. Dankowicz and Nordmark [20] considered a dry friction oscillator and showed that the map in this case will have a power of 3/2 term in one side which gives it some special features. To illustrate, consider the map

$$x_{n+1} = \begin{cases} ax_n + \mu & \text{if } x_n \leqslant 0, \\ ax_n - bx_n^{3/2} + \mu & \text{if } x_n \geqslant 0. \end{cases} \tag{2}$$

This map is continuous at the border $x_n = 0$, and there is no discontinuity in the slope either. This implies that even though the function is represented piecewise, it is continuous and smooth. This property has come to be known as the "3/2 singularity" even though it is not really a singularity.

Molenaar et al. [21] re-analysed the impact oscillator with a hard wall and a compliant wall, and showed that the map takes the functional form

$$\begin{aligned} x_{n+1} &= a_1 x_n + y_n + \rho \\ y_{n+1} &= -a_2 x_n \end{aligned} \Bigg\} \quad \text{if } x_n \leqslant 0,$$
$$\begin{aligned} x_{n+1} &= \pm\sqrt{x_n} + b_1 x_n + y_n + \rho \\ y_{n+1} &= b_2 x_n \end{aligned} \Bigg\} \quad \text{if } x_n \geqslant 0. \tag{3}$$

The map differs in three ways from the Nordmark map: (a) the sign of square-root term, which is negative for the instantaneous impact and positive for non-instantaneous impact, (b) the inclusion of the term $b_1 x_n$, and (c) the dependence of the coefficient b_2 on the system parameters, which is different from that of the parameter d of (1). Molenaar et al. concluded that square-root singularity survives in the system with the compliant wall, and hence a similar bifurcation sequence is observed in systems with hard wall as well as compliant wall.

Subsequently di Bernardo et al. [22,23] analysed various types of non-smooth mechanical systems allowing grazing condition. They showed that if the flows at the two sides of the switching surface are different, the map will have a square-root singularity; and if the flows in the immediate vicinity of the switching surface are the same (but the first or the second derivative of the flow are different) then it results in a 3/2 singularity in the map.

The hard impact oscillator, in which the state itself undergoes a discontinuous jump at the impacting condition, obviously belongs to the first category. The soft impact oscillator with cushion provided by only an unstressed spring (and no damper) is an example of the second type. But soft impacting systems with prestressed spring and/or a damper in the cushion constitutes the twilight zone between the two types.

It has been shown by Ma et al. [24] that in such systems the determinant of the Jacobian matrix remains the same in the immediate neighbourhood of the grazing condition and the trace shows the square-root singularity. But that raises fresh questions. What are the effects of the individual components of the cushion (spring constant, friction, and prestressing) on the character of the map at the two sides of the border? One can imagine smoothly changing the relevant parameters to transform one type of system into another. The question is, how does a map with 3/2 singularity smoothly change into that with a square-root singularity? What is the behaviour of the map away from the borderline representing the grazing condition? In this paper we probe these questions—both numerically as well as experimentally.

The system considered in this paper consists of a mass M supported by a spring k_1 and a damper R_1 attached to a rigid wall (Fig. 1). There is a sinusoidally varying force $F \cos \omega t$ acting on the mass.
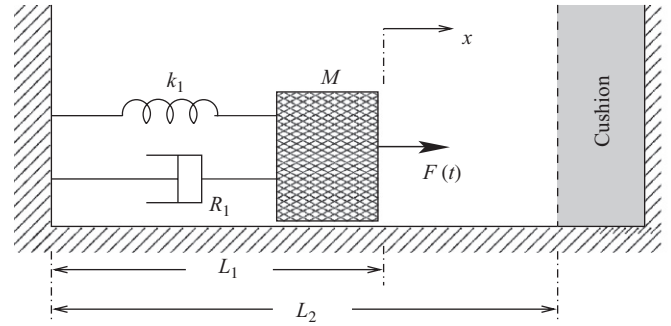

Fig. 1. The soft impacting oscillator system considered in this paper.

When the spring is relaxed, the right end of the mass is at a distance L_1 from the wall, and x is the elongation from the unstretched position. On the other side there is a wall with a cushion at distance L_2 provided to soften the impact. The character of the vector field at the two sides of the switching surface depends on the nature of the cushion.

We probe the bifurcations occurring when the trajectory grazes the boundary between non-impacting state and the impacting state. The discrete observations are done in synchronism with the external periodic input, to obtain a "stroboscopic sampling." It is known that such switching dynamical systems yield maps that are piecewise smooth. We are interested in the character of the two-dimensional discrete map at the two sides of the borderline.

It is convenient to express the local linear behaviour in the normal form [25–27]

$$\begin{bmatrix} x_{n+1} \\ y_{n+1} \end{bmatrix} = \begin{bmatrix} \tau & 1 \\ -\delta & 0 \end{bmatrix} \begin{bmatrix} x_n \\ y_n \end{bmatrix} + \mu \begin{bmatrix} 1 \\ 0 \end{bmatrix} \tag{4}$$

which is expressed in terms of only two parameters: the trace τ and the determinant δ of the Jacobian matrix. We investigate how the trace and the determinant change as the system is driven from the non-impacting state to the impacting state by continuous variation of the parameter.

We first probe the character of the normal form using an experimental set-up where the cushioning surface contains a spring, and no damper. In case of unstressed spring, this configuration causes the vector field to be identical in the immediate neighbourhood of the switching surface, and can be considered a testing ground for the theory of the 3/2 singularity.

Then we consider four different types of cushion to illustrate the different types of change in the vector field across the switching surface. Since it is difficult to set up the experimental system for all the configurations, this part of the study is conducted through numerical means.

We show that the normal form representation of the Poincaré map has very definite characteristic features depending on the properties of the vector field at the two sides of the borderline.

2. The experimental set-up

An experimental oscillator developed at the University of Aberdeen [17,28,29] was used for the purpose of this investigation. It consists of a block of mild steel supported by parallel leaf springs which allow displacement of the mass without rotation (Fig. 2). The secondary spring is made from spring steel, with the point of contact being accurately located via an adjustable screw. The harmonic excitation was achieved using an electro-dynamic shaker. Accelerometers were mounted on the base and on the oscillator, and an eddy current displacement transducer was mounted over one leaf spring

(a)

(b)
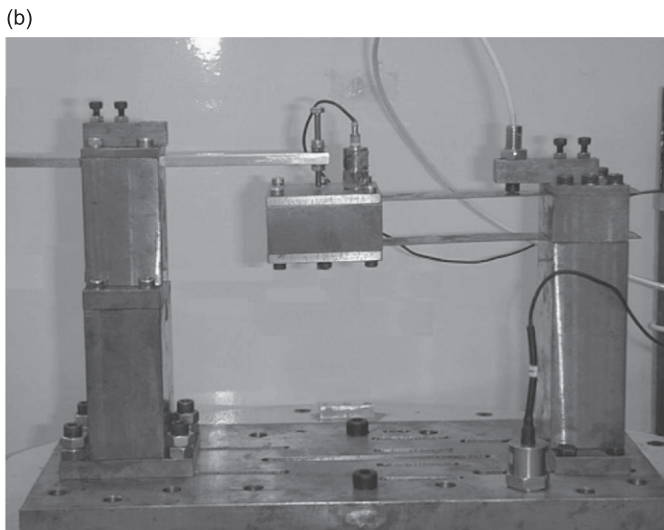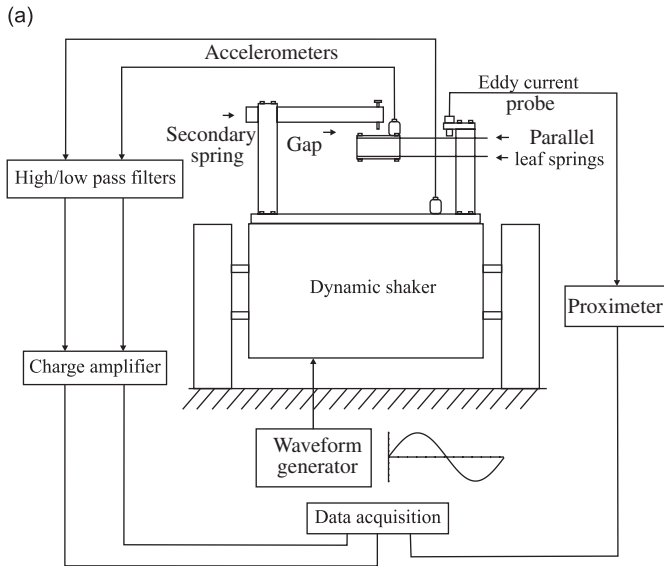
Fig. 2. The experimental set-up: (a) the schematic diagram, and (b) photograph of the physical system. Parallel leaf springs ensure displacement without rotation. Harmonic excitation is achieved via the base. Detailed description of the set-up can be found in [28,29].

in order to measure the position of the mass under the assumption of small displacements. Within free vibration, a natural frequency of 11 Hz and damping of $2.18 \, \text{kg s}^{-1}$ were determined using the logarithmic decrements method. The stiffness ratio of the secondary to primary springs was measured under static displacement as 1.29. The base mounted accelerometer allowed determination of the amplitude of excitation from the relationship $\ddot{x}_{max} = F\omega^2$. The data were low pass filtered with a cutoff frequency of 100 Hz before being amplified by the hardware. The data acquisition was performed using LABVIEW, with a scan rate of 1000 samples per second (approximately 150 per period of forcing). The data was smoothed with a Savitsky–Golay method, using a second order polynomial fit around 21 data points. Stroboscopic sampling was obtained by means of a linear interpolation between the closest data points, since in general there was not an integer number of data points per period of excitation.

For a suitably chosen forcing amplitude and frequency, we obtain a non-impacting orbit. As the amplitude is increased, the fixed point moves in position, and at a specific parameter value it collides with the border. This fixed point corresponds to the continuous-time orbit that just grazes the switching surface. As the parameter is further varied, the orbit becomes impacting. The problem was to experimentally determine the Jacobian matrix of the period-1 orbit as the parameter is varied through the value corresponding to the grazing condition. It was done in the same manner as in [29], and is briefly described below.

Mathematically speaking, for the perturbation about a fixed point of the stroboscopic map, $\mathbf{v}^* = P(\mathbf{v}^*)$, we can write

$$\mathbf{u}_{n+1} = (\mathbf{v} - \mathbf{v}^*)_{n+1} = \left.\frac{\partial P}{\partial \mathbf{x}}\right|_{\mathbf{v}=\mathbf{v}^*} (\mathbf{v} - \mathbf{v}^*)_n + O(\mathbf{u}_n^2) \tag{5}$$

where the derivative matrix is the Jacobian. Experimentally this meant waiting for a trajectory with arbitrary initial conditions to become close to a stable limit cycle, and then giving the oscillator a small "kick" to perturb the trajectory, taking care that close to grazing, a non-impacting trajectory was not perturbed into a impacting trajectory, or vice-versa. A number of Poincaré points before the perturbation were averaged and subtracted from the data after the perturbation, so that for a given point the linear map $\mathbf{u}_{n+1} = \mathbf{A}\mathbf{u}_n$ provides a good estimation of the next point. Care was needed to ensure that the strength of perturbation was sufficiently large so that the transients could be detected above the experimental noise, but small enough to preserve the local nature of the linear maps.

(a)　　　　　　　　　　　　　　　　(b)
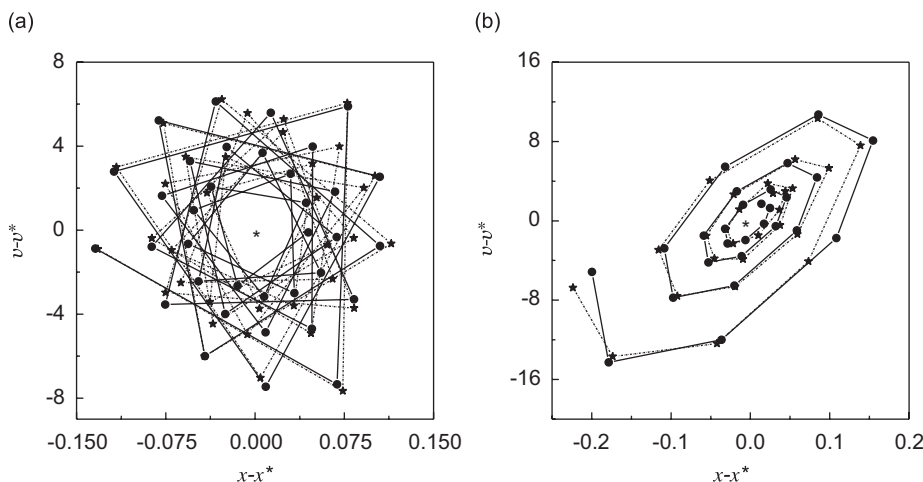
Fig. 3. Transients in the stroboscopic map for (a) 6.3 Hz (before contact) and (b) 6.9 Hz (after contact). Experimental points are shown by black stars whereas linear map fit by black circles. The linear map is a very good model for quite large perturbations, as evidenced by accuracy of the fit.
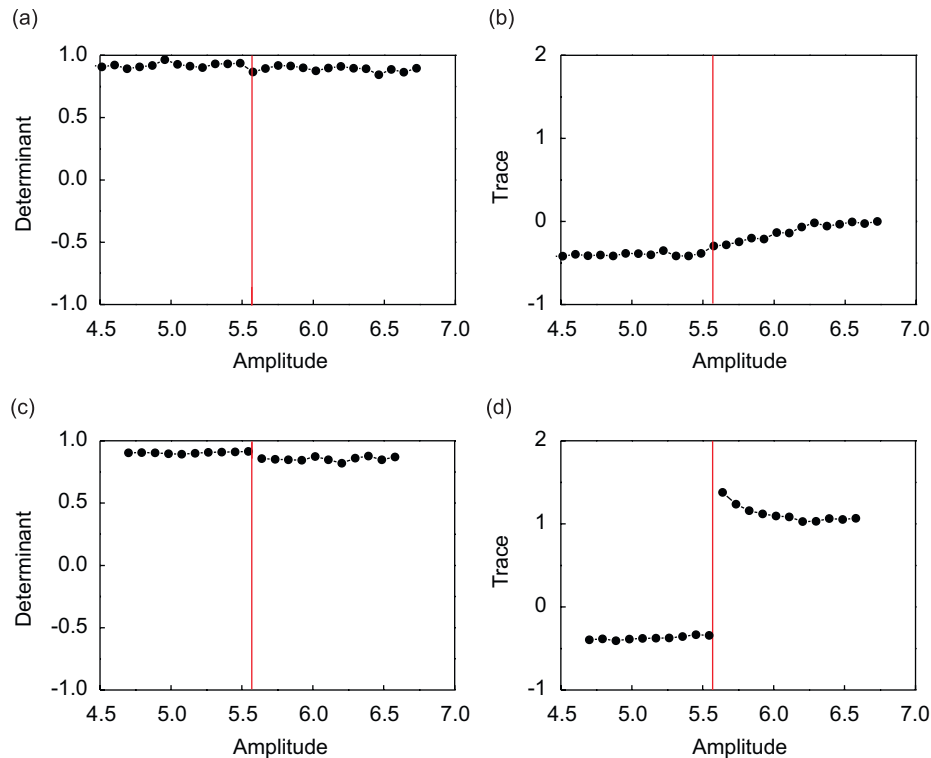
Fig. 4. Results for the experimental system: the variation of determinant and trace, with the variation of the forcing amplitude. Two cases are presented: (a) and (b) for an unprestressed spring; (c) and (d) for a spring with prestress.

Successively large perturbations were tested for deviation from linearity until a suitable one was found. Only three points are required to determine all four Jacobian elements, but in practice between 5 and 10 were used in order to reduce the effects of noise and as a test of the validity of the method. A conjugate gradient method was used to minimize a least squares fit of the linear map to the data. Fig. 3 gives two examples of these fits, both before and after impact. In all cases tested, the eigenvalues were complex conjugates, hence there were no real eigenvectors and the transients were rotated about the fixed point.

The results obtained from the experiment are presented in Fig. 4, where the parameters of the normal form (4) are estimated for different values of the excitation amplitude F. Experimental points are shown as black dots joined by a line where the response in between is clearly understood. The figure shows that while the system is driven from the non-impacting state to the impacting state, the determinant of the Jacobian matrix remains almost constant.

In the case of the unprestressed spring (Figs. 4(a) and (b)), the trace is clearly continuous across the grazing boundary, which is indicated by the vertical line. Since the normal form of the map is the same at the two sides of the grazing condition, the experiment showed that the map is smooth and continuous, as expected from a "power-of-3/2" character.

In the case of the prestressed spring (Figs. 4(c) and (d)), the trace, after grazing, is vastly changed and returns smoothly to a smaller value. This is consistent with a square-root singularity at the grazing point. However, very close to the grazing condition, we observed noise-induced chaotic motion, due to which reliable data could not be obtained. This explains the absence of very large values of the trace very close to grazing. For this we need to resort to simulation of the various configurations of the system considered.

3. The method of numerical investigation

We now systematically study the effect of variation of the vector fields at the two sides of the border. We have adopted a specific method for the numerical study, and so a description about the method is in order.

3.1. Solution flow and Poincaré map

A switching system with non-autonomous subsystems is usually described by equations of the form

$$S_1 : \dot{\mathbf{x}} = f_1(t, \mathbf{x}, p_1) \quad \text{if } \mathbf{x} \in M_1,$$
$$S_2 : \dot{\mathbf{x}} = f_2(t, \mathbf{x}, p_2) \quad \text{if } \mathbf{x} \in M_2. \tag{6}$$

where $\mathbf{x} \in \mathbb{R}^n$ are the state variables, $p_{1,2}$ are the system parameters, f_1 and f_2 are the governing functions of sub-system S_1 and S_2 when the solution moves in sub-space M_1 and M_2, respectively. The functions $f_{1,2}$ contain time explicitly.

We assume that the sub-spaces M_1 and M_2 are two separated parts of one space. That means they have no intersection and are divided by a common border B defined only by states

$$B = \{\mathbf{x} \in \mathbb{R}^n : \beta(\mathbf{x}) = 0\}, \tag{7}$$

where $\beta(\mathbf{x})$ is the border function.

Thus, the two sub-spaces are given by

$$M_1 = \{\mathbf{x} \in \mathbb{R}^n : \beta(\mathbf{x}) \geqslant 0\},$$
$$M_2 = \{\mathbf{x} \in \mathbb{R}^n : \beta(\mathbf{x}) \leqslant 0\}. \tag{8}$$

The solution of the system is governed by the functions f_1 and f_2 as given in (6), depending on whether the state is in M_1 or in M_2. We express the solution functions as

$$\mathbf{x}(t) = \varphi_1(t, t_0, \mathbf{x}_{01}) \quad \text{if } \mathbf{x} \in M_1,$$

$$\mathbf{x}(t) = \varphi_2(t, t_0, \mathbf{x}_{02}) \quad \text{if } \mathbf{x} \in M_2, \tag{9}$$

where $\mathbf{x}_{01}$ and $\mathbf{x}_{02}$ are the initial conditions, and t_0 is the starting time.

We assume that both $f_1(t, \mathbf{x}, p_1)$ and $f_2(t, \mathbf{x}, p_2)$ are periodic functions with identical period T, i.e.,

$$f_{1,2}(t, \mathbf{x}, p_{1,2}) = f_{1,2}(t + T, \mathbf{x}, p_{1,2}). \tag{10}$$

Now, define the stroboscopic mapping as

$$F_m : \mathbb{R}^n \to \mathbb{R}^n; \quad \mathbf{x}(0) \mapsto \mathbf{x}(T). \tag{11}$$

In this map, if a solution satisfies $\mathbf{x}(0) = \mathbf{x}(kT) \neq \mathbf{x}(jT), k = 1, 2, \ldots; 0 < j < k$, it is a period-$k$ solution.

In a periodically forced system, the stroboscopic sampling points will not generally lie on the switching manifold. Suppose there is a solution flow in one period as follows.

1. Starting at $\mathbf{x}_0 \in M_1$, the state moves in M_1 until the solution satisfies the switching condition B at $\mathbf{x}_1$ after time τ_1.
2. Crossing the border B, the state moves into M_2. Then at time τ_2, the solution flow crosses the switching manifold again at $\mathbf{x}_2$, and returns to sub-space M_1.
3. Finally, the state reaches $\mathbf{x}_3$ after time T.

According to (9) and (7), the above solution flow can be described as

$$\mathbf{x}_1 = \varphi_1(\tau_1, \tau_0, \mathbf{x}_0) \quad \text{first interval when } \mathbf{x} \in M_1; \tag{12}$$

$$\mathbf{x}_2 = \varphi_2(\tau_2, \tau_1, \mathbf{x}_1) \quad \text{second interval when } \mathbf{x} \in M_2; \tag{13}$$

$$\mathbf{x}_3 = \varphi_1(T + \tau_0, \tau_2, \mathbf{x}_2) \quad \text{solution returns to } \mathbf{x}_0; \tag{14}$$

$$\beta(\mathbf{x}_1) = 0 \quad \text{point } \mathbf{x}_1 \text{ is on the switching manifold}; \tag{15}$$

$$\beta(\mathbf{x}_2) = 0 \quad \text{point } \mathbf{x}_2 \text{ is also on the switching manifold}. \tag{16}$$

This is shown schematically in Fig. 5. Since we are considering a periodic solution, the starting time can be regarded as zero from the analytical viewpoint. Without loss of generality, we will set $\tau_0 = 0$ in the following text.

3.2. Obtaining the fixed point

The behaviour of periodic solution flow of the system is reduced to the behaviour of fixed points of the map, $F_m : \mathbf{x}_0 \mapsto \mathbf{x}_3$. In this section, we will introduce the method to obtain the location of the fixed point.

A fixed point exists if $\mathbf{x}(0) = \mathbf{x}(T)$, i.e., if $\mathbf{x}_0 = \mathbf{x}_3$. To determine a periodic solution, we have $3n+2$ scalar unknowns $\mathbf{y} = \{\mathbf{x}_0, \mathbf{x}_1, \mathbf{x}_2, \tau_1, \tau_2\}$. Meanwhile, there are $3n+2$ scalar equations in (12)–(16), which can be rewritten as

$$G_{1,n}(\mathbf{y}) = \mathbf{x}_1 - \varphi_1(\tau_1, 0, \mathbf{x}_0) = 0, \tag{17}$$

$$G_{n+1,2n}(\mathbf{y}) = \mathbf{x}_2 - \varphi_2(\tau_2, \tau_1, \mathbf{x}_1) = 0, \tag{18}$$

$$G_{2n+1,3n}(\mathbf{y}) = \mathbf{x}_0 - \varphi_1(T, \tau_2, \mathbf{x}_2) = 0, \tag{19}$$
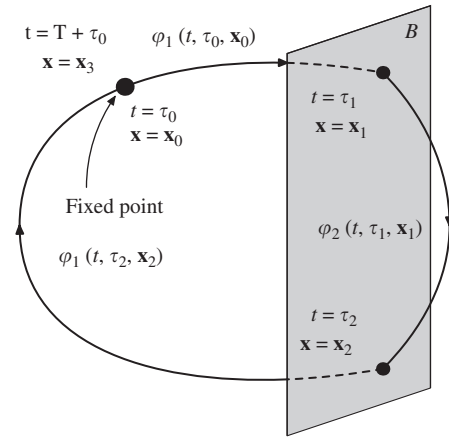

$$t = T + \tau_0 \qquad \varphi_1(t, \tau_0, \mathbf{x}_0)$$
$$\mathbf{x} = \mathbf{x}_3$$

Fig. 5. A period-1 orbit, and its Poincaré map $\mathbf{x}_0 \mapsto \mathbf{x}_3$.

$$G_{3n+1}(\mathbf{y}) = \beta(\mathbf{x}_1) = 0, \tag{20}$$

$$G_{3n+2}(\mathbf{y}) = \beta(\mathbf{x}_2) = 0. \tag{21}$$

In general, the solutions may not be available in closed form. We therefore have to solve the above equation sets using appropriate numerical method. For this purpose, we have used Newton's method, such that

$$\mathbf{y}_{k+1} = \mathbf{y}_k - \frac{G(\mathbf{y}_k)}{G'(\mathbf{y}_k)}, \quad k = 0, 1, \ldots, \tag{22}$$

where $G'(\mathbf{y}_k)$ is the partial derivatives $\partial G(\mathbf{y}_k)/\partial \mathbf{y}_k$ of the solution with respect to the unknowns for each step. It can be obtained as

$$\frac{\partial G(\mathbf{y})}{\partial \mathbf{y}} = \begin{bmatrix} \dfrac{\partial G_{1,n}(\mathbf{y})}{\partial \mathbf{y}} \\[4pt] \dfrac{\partial G_{n+1,2n}(\mathbf{y})}{\partial \mathbf{y}} \\[4pt] \dfrac{\partial G_{2n+1,3n}(\mathbf{y})}{\partial \mathbf{y}} \\[4pt] \dfrac{\partial G_{3n+1}(\mathbf{y})}{\partial \mathbf{y}} \\[4pt] \dfrac{\partial G_{3n+2}(\mathbf{y})}{\partial \mathbf{y}} \end{bmatrix}$$

$$= \begin{bmatrix} -\dfrac{\partial \varphi_1(\tau_1)}{\partial \mathbf{x}_0} & \vdots & \mathbf{I}_n & \vdots & \mathbf{O}_{n,n} & \vdots & -\dfrac{\partial \varphi_1(\tau_1)}{\partial \tau_1} & \vdots & \mathbf{O}_{n,1} \\[6pt] \mathbf{O}_{n,n} & \vdots & -\dfrac{\partial \varphi_2(\tau_2)}{\partial \mathbf{x}_1} & \vdots & \mathbf{I}_n & \vdots & -\dfrac{\partial \varphi_2(\tau_2)}{\partial \tau_1} & \vdots & -\dfrac{\partial \varphi_2(\tau_2)}{\partial \tau_2} \\[6pt] \mathbf{I}_n & \vdots & \mathbf{O}_{n,n} & \vdots & -\dfrac{\partial \varphi_1(T)}{\partial \mathbf{x}_2} & \vdots & \mathbf{O}_{n,1} & \vdots & -\dfrac{\partial \varphi_1(T)}{\partial \tau_2} \\[6pt] \mathbf{O}_{1,n} & \vdots & \dfrac{\partial \beta(\mathbf{x}_1)}{\partial \mathbf{x}_1} & \vdots & \mathbf{O}_{1,n} & \vdots & 0 & \vdots & 0 \\[6pt] \mathbf{O}_{1,n} & \vdots & \mathbf{O}_{1,n} & \vdots & \dfrac{\partial \beta(\mathbf{x}_2)}{\partial \mathbf{x}_2} & \vdots & 0 & \vdots & 0 \end{bmatrix}, \tag{23}$$

where $\mathbf{I}_n$ is an identity matrix with order n, and $\mathbf{O}_{i,j}$ indicate zero matrix with i rows and j columns. Moreover, the shorter notations used here mean

$$\varphi_1(\tau_1) \mapsto \varphi_1(\tau_1, 0, \mathbf{x}_0); \quad \varphi_2(\tau_2) \mapsto \varphi_2(\tau_2, \tau_1, \mathbf{x}_1);$$

$$\varphi_1(T) \mapsto \varphi_1(T, \tau_2, \mathbf{x}_2). \tag{24}$$

Now, let us look at the terms in (23), which need to be known in order to apply the Newton algorithm. The partial derivatives of the

solution flow with respect to time can be written as

$$\frac{\partial \varphi_1(\tau_1)}{\partial \tau_1} = \left. \frac{\partial \varphi_1(t, 0, \mathbf{x}_0)}{\partial t} \right|_{t=\tau_1} = f_1(\tau_1, \mathbf{x}_1, p_1), \tag{25}$$

$$\frac{\partial \varphi_2(\tau_2)}{\partial \tau_2} = \left. \frac{\partial \varphi_2(t, \tau_1, \mathbf{x}_1)}{\partial t} \right|_{t=\tau_2} = f_2(\tau_2, \mathbf{x}_2, p_2). \tag{26}$$

On the other hand, partial derivatives of the solution flow with respect to the *initial time points* τ_1 and τ_2 [30] are

$$\frac{\partial \varphi_2(\tau_2)}{\partial \tau_1} = \frac{\partial \varphi_2(\tau_2, \tau_1, \mathbf{x}_1)}{\partial \tau_1} = -\frac{\partial \varphi_2(\tau_2, \tau_1, \mathbf{x}_1)}{\partial \mathbf{x}_1} f_2(\tau_1, \mathbf{x}_1, p_2), \tag{27}$$

$$\frac{\partial \varphi_1(T)}{\partial \tau_2} = \frac{\partial \varphi_1(T, \tau_2, \mathbf{x}_2)}{\partial \tau_2} = -\frac{\partial \varphi_1(T, \tau_2, \mathbf{x}_2)}{\partial \mathbf{x}_2} f_1(\tau_2, \mathbf{x}_2, p_1). \tag{28}$$

Next, we need to obtain the values of $\partial \varphi_1(\tau_1)/\partial \mathbf{x}_0$, $\partial \varphi_2(\tau_2)/\partial \mathbf{x}_1$, and $\partial \varphi_1(T)/\partial \mathbf{x}_2$. These partial derivatives of the solution functions with respect to the initial conditions are obtained by solving the differential equations or linear variational equations [30]:

$$\frac{d}{dt}\left(\frac{\partial \varphi_1(\tau_1)}{\partial \mathbf{x}_0}\right) = \frac{\partial f_1}{\partial \mathbf{x}}\left(\frac{\partial \varphi_1(\tau_1)}{\partial \mathbf{x}_0}\right), \quad \left. \frac{\partial \varphi_1(\tau_1)}{\partial \mathbf{x}_0} \right|_{t=0} = \mathbf{I}^n, \tag{29}$$

$$\frac{d}{dt}\left(\frac{\partial \varphi_2(\tau_2)}{\partial \mathbf{x}_1}\right) = \frac{\partial f_2}{\partial \mathbf{x}}\left(\frac{\partial \varphi_2(\tau_2)}{\partial \mathbf{x}_1}\right), \quad \left. \frac{\partial \varphi_2(\tau_2)}{\partial \mathbf{x}_1} \right|_{t=\tau_1} = \mathbf{I}^n, \tag{30}$$

$$\frac{d}{dt}\left(\frac{\partial \varphi_1(T)}{\partial \mathbf{x}_2}\right) = \frac{\partial f_1}{\partial \mathbf{x}}\left(\frac{\partial \varphi_1(T)}{\partial \mathbf{x}_2}\right), \quad \left. \frac{\partial \varphi_1(T)}{\partial \mathbf{x}_2} \right|_{t=\tau_2} = \mathbf{I}^n. \tag{31}$$

Finally, $\left. \frac{\partial \beta}{\partial \mathbf{x}} \right|_{\mathbf{x}=\mathbf{x}_1, \mathbf{x}_2}$ have to be written in a right form. Because the border function $\beta(\mathbf{x}) = 0$ is a one-dimensional equation, $\partial \beta/\partial \mathbf{x}$ is just a $1 \times n$ matrix, whose elements are derivatives with respect to each variable of $\mathbf{x}$.

Now we can evaluate every element of the matrix in (23) for a given $\mathbf{x}$. By choosing good initial values and using Newton's iterations, we can converge to the fixed point. In each step, the elements of the matrix in (23) are updated depending on the current value of $\mathbf{x}$. Thus, while the procedure converges on the fixed point, the elements of the matrix in (23) also converge onto the values corresponding to the fixed point.

3.3. Obtaining the Jacobian matrix at the fixed point

In this section we show how the information about the stability of the fixed point can be extracted from the elements of the matrix in (23). From (12)–(14) we can write

$$\frac{\partial \mathbf{x}_1}{\partial \mathbf{x}_0} = \frac{\partial \varphi_1(\tau_1)}{\partial \tau_1}\frac{\partial \tau_1}{\partial \mathbf{x}_0} + \frac{\partial \varphi_1(\tau_1)}{\partial \mathbf{x}_0}, \tag{32}$$

$$\frac{\partial \mathbf{x}_2}{\partial \mathbf{x}_0} = \frac{\partial \varphi_2(\tau_2)}{\partial \tau_2}\frac{\partial \tau_2}{\partial \mathbf{x}_0} + \frac{\partial \varphi_2(\tau_2)}{\partial \tau_1}\frac{\partial \tau_1}{\partial \mathbf{x}_0} + \frac{\partial \varphi_2(\tau_2)}{\partial \mathbf{x}_1}\frac{\partial \mathbf{x}_1}{\partial \mathbf{x}_0}, \tag{33}$$

$$\frac{\partial \mathbf{x}_3}{\partial \mathbf{x}_0} = \frac{\partial \varphi_1(T)}{\partial \tau_2}\frac{\partial \tau_2}{\partial \mathbf{x}_0} + \frac{\partial \varphi_1(T)}{\partial \mathbf{x}_2}\frac{\partial \mathbf{x}_2}{\partial \mathbf{x}_0}. \tag{34}$$

Substituting (25), (26) and (27), (28) into (32)–(34), we get

$$\frac{\partial \mathbf{x}_1}{\partial \mathbf{x}_0} = f_1(\tau_1, \mathbf{x}_1, p_1)\frac{\partial \tau_1}{\partial \mathbf{x}_0} + \frac{\partial \varphi_1(\tau_1)}{\partial \mathbf{x}_0}, \tag{35}$$

$$\frac{\partial \mathbf{x}_2}{\partial \mathbf{x}_0} = f_2(\tau_2, \mathbf{x}_2, p_2)\frac{\partial \tau_2}{\partial \mathbf{x}_0} - \frac{\partial \varphi_2(\tau_2)}{\partial \mathbf{x}_1}f_2(\tau_1, \mathbf{x}_1, p_2)\frac{\partial \tau_1}{\partial \mathbf{x}_0} + \frac{\partial \varphi_2(\tau_2)}{\partial \mathbf{x}_1}\frac{\partial \mathbf{x}_1}{\partial \mathbf{x}_0}, \tag{36}$$

$$\frac{\partial \mathbf{x}_3}{\partial \mathbf{x}_0} = -\frac{\partial \varphi_1(T)}{\partial \mathbf{x}_2}f_1(\tau_2, \mathbf{x}_2, p_1)\frac{\partial \tau_2}{\partial \mathbf{x}_0} + \frac{\partial \varphi_1(T)}{\partial \mathbf{x}_2}\frac{\partial \mathbf{x}_2}{\partial \mathbf{x}_0}. \tag{37}$$

Note that (37) gives the Jacobian matrix of the Poincaré map $\mathbf{x}_0 \mapsto \mathbf{x}_3$, which is needed in order to analyse the stability property.

To evaluate (35)–(37), we also need the partial derivatives of the evolution times within each sub-system with respect to the initial condition. Since the times of evolution within each sub-system is determined by the switching condition, these partial derivatives can be obtained from the expressions of the switching manifolds. From (15) and (16) we can write

$$\frac{\partial \beta(\mathbf{x}_1)}{\partial \mathbf{x}_0} = \frac{\partial \beta}{\partial \mathbf{x}}\frac{\partial \mathbf{x}_1}{\partial \mathbf{x}_0} = 0 \quad \text{and}$$

$$\frac{\partial \beta(\mathbf{x}_2)}{\partial \mathbf{x}_0} = \frac{\partial \beta}{\partial \mathbf{x}}\frac{\partial \mathbf{x}_2}{\partial \mathbf{x}_0} = 0. \tag{38}$$

As described at the end of Section 3.2, $\beta(\mathbf{x}) = 0$ is a one-dimensional equation. For example, when $\beta(\mathbf{x})$ is in a simple form like $\mathbf{x}(1) =$ constant, $\partial \beta/\partial \mathbf{x} = [1, 0, \ldots, 0]$. Thus, if $\partial \beta/\partial \mathbf{x} \cdot \partial \mathbf{x}_1/\partial \mathbf{x}_0 = 0$ as given by (38), the corresponding first row of $\partial \mathbf{x}_1/\partial \mathbf{x}_0$ must be $[0, \ldots, 0]$. But if the switching manifold is given by an equation involving more than one state variable like the form $\beta(\mathbf{x}) = \mathbf{x}(1) - \mathbf{x}(2) = 0$, then $\partial \beta/\partial \mathbf{x} = [1, -1, 0, \ldots, 0]$. Thus the difference between the first two rows of $\partial \mathbf{x}_1/\partial \mathbf{x}_0$ will be zero. Anyway, $\partial \beta/\partial \mathbf{x}$ supplies the additional information of specific dimension(s) related to border function, by which we can solve the partial derivatives of the times of evolution with respect to the initial state $\mathbf{x}_0$. Substituting (35) and (36) into (38), we get

$$\frac{\partial \tau_1}{\partial \mathbf{x}_0} = -\frac{(\partial \beta/\partial \mathbf{x})((\partial \varphi_1(\tau_1))/\partial \mathbf{x}_0)}{(\partial \beta/\partial \mathbf{x})f_1(\tau_1, \mathbf{x}_1, p_1)} \quad \text{and}$$

$$\frac{\partial \tau_2}{\partial \mathbf{x}_0} = \frac{\frac{\partial \beta}{\partial \mathbf{x}}\frac{\partial \varphi_2(\tau_2)}{\partial \mathbf{x}_1}\frac{\partial \mathbf{x}_1}{\partial \mathbf{x}_0} - \frac{\partial \beta}{\partial \mathbf{x}}\frac{\partial \varphi_2(\tau_2)}{\partial \mathbf{x}_1}f_2(\tau_1, \mathbf{x}_1, p_2)\frac{\partial \tau_1}{\partial \mathbf{x}_0}}{\frac{\partial \beta}{\partial \mathbf{x}}f_2(\tau_2, \mathbf{x}_2, p_2)}. \tag{39}$$

These expressions, substituted into (37), give the Jacobian matrix $\partial \mathbf{x}_3/\partial \mathbf{x}_0$ of the Poincaré map. Then by finding the eigenvalues, we can determine the stability of specific fixed point, i.e., of the corresponding periodic orbit in continuous time.

Thus, all the terms necessary to obtain the Jacobian matrix are derived in the process of finding the fixed point, and hence the Jacobian of the fixed point can be obtained with very little additional computational burden. We only need to substitute the right terms into the right places.[1] A separate program was

---

[1] In this paper we are considering only period-1 orbits. For higher periodic orbits, the solution flow can be formulated according to the time instants at which the flow crosses the border or reaches the sampling time nT. The process will only involve a larger number of equations of the form (12)–(16). Therefore, to compute a complicated orbit we will only need to solve a larger number of simultaneous algebraic equations for a larger number of unknowns. An effective numerical method can solve them and can find the position of the fixed point without much difficulty. Note that for a period-n fixed point, the Jacobian matrix is to be composed by multiplying the Jacobian matrices corresponding to each period in the orbit.

written where one can give an initial condition and compute the orbit for one (or an integer multiple) period of the external forcing function. If the final state comes close to the initial state, *that* position is taken as the initial value for the Newton–Raphson routine.

4. Different types of soft impacting systems

In this section we consider four different types of the cushion, resulting in different characteristic transitions of the vector field from one side of the switching surface to the other. Since the distance of the fixed point from the borderline is directly dependent on the forcing amplitude, in the following study we take F as the bifurcation parameter. For each value of the parameter F, we obtain the fixed point—irrespective of whether it is stable or unstable—and the trace and the determinant of the Jacobian matrix, which are then plotted against F.

4.1. System A

We start with a system similar to the one in the experimental set-up, where the cushion in front of the wall has only an unstressed spring with spring constant k_2, and no mass or frictional element, as shown in Fig. 6. In the unstressed position, the impacting surface is at a distance L_2 from the wall.
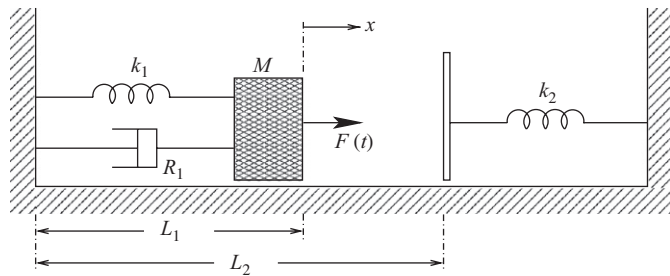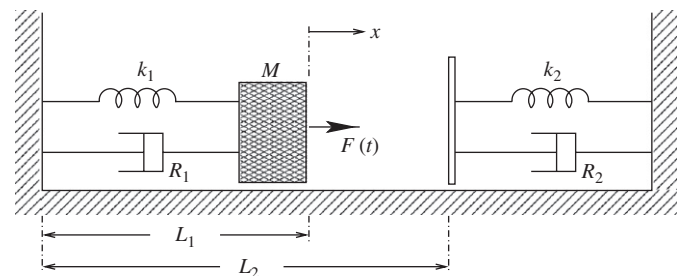
If $x + L_1 < L_2$ then it is a simple harmonic oscillator given by the equation

$$M\ddot{x} + R_1\dot{x} + k_1 x = F\cos\omega t. \tag{40}$$

We call it Subsystem-1.

If $x + L_1 \geqslant L_2$ then a soft impact occurs, following which the system equation changes to

$$M\ddot{x} + R_1\dot{x} + k_1 x + k_2(L_1 + x - L_2) = F\cos\omega t. \tag{41}$$

We call it Subsystem-2.

When an impact occurs, the term $k_2(L_1 + x - L_2)$ is zero, and so the vector field in the immediate neighbourhood of the switching manifold at the two sides are the same.

The results showing the variation of the trace and the determinant of the Jacobian matrix with the forcing amplitude are given in Fig. 7.

It is noticeable that the determinant remains invariant over a large range of the parameter, and the trace is continuous across the grazing condition. However, the trace changes very fast subsequently, and the derivative of the trace with respect to the parameter seems to have a square-root type singularity. If the parameter at which grazing takes place is denoted as F_g, then the derivative of the trace with respect to the parameter tends to ∞ as $F \to F_g^+$. These results are supported by the experiment reported in Section 2.

Fig. 6. Schematic diagram of the System-A.

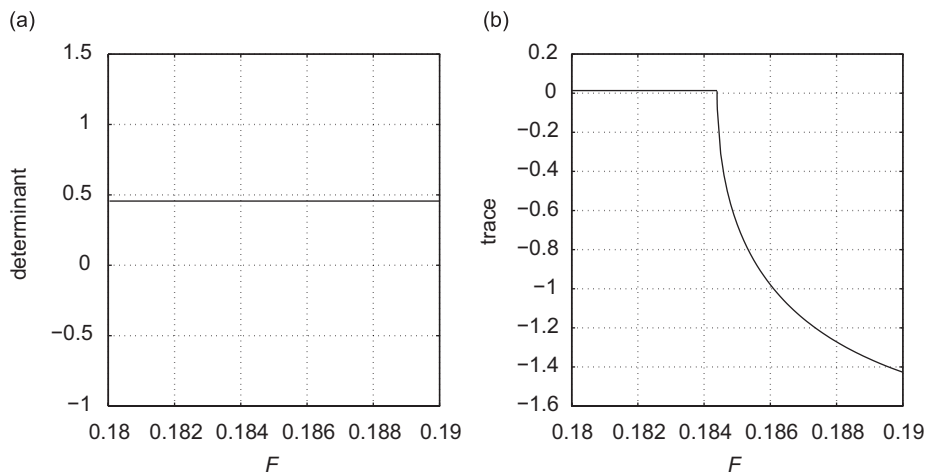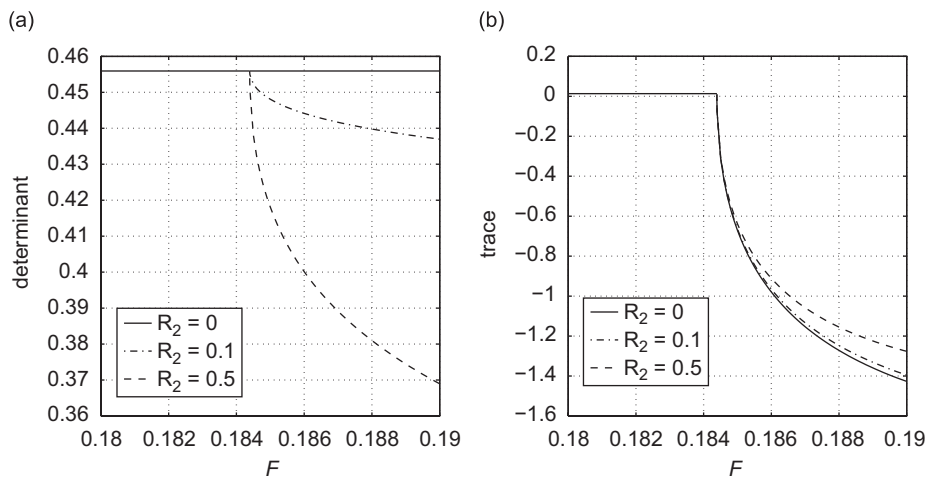Fig. 8. Schematic diagram of the System-B.

Fig. 7. The variation of (a) determinant and (b) trace of the Jacobian matrix of System-A as F is varied through the grazing condition. The parameters in normalized units are $M = 1$, $k_1 = k_2 = 1$, $L_2 - L_1 = 0.5$, $R_1 = 0.1$, $\omega = 0.8$.

(a)

(b)

Fig. 9. The variation of (a) determinant and (b) trace of the Jacobian matrix of System-B as F is varied through the grazing condition. The parameters are $M = 1$, $k_1 = 1$, $L_2 - L_1 = 0.5$, $\omega = 0.8$, $R_1 = 0.1$. R_2 is varied in steps.

4.2. System B

Now we consider the system which has a damper (R_2) along with the spring k_2 in the cushioning surface as shown in Fig. 8. Subsystem-1 remains unaltered, and Subsystem-2 changes to

$$M\ddot{x} + (R_1 + R_2)\dot{x} + k_1 x + k_2(L_1 + x - L_2) = F\cos\omega t. \tag{42}$$

In this case the mass disengages from the cushion when the contact force becomes zero, i.e., when $k_2(L_1 + x - L_2) + R_2\dot{x} = 0$. As an impact occurs, the damper reacts with a force $R_2\dot{x}$, and therefore the vector field at the two sides of the switching surface are not the same. However, when grazing occurs at zero velocity, this term is zero, and hence in the immediate neighbourhood of the grazing point $(x = L_2 - L_1, \dot{x} = 0)$ the vector field is smooth.

The results for this system is given in Fig. 9. The main difference caused by the damper is the change in the determinant following the grazing condition. Even though the determinant is continuous across the grazing condition, it shows a sharp gradient following the transition into impacting state, which depends on the value of R_2. The change observed in the trace is only a quantitative shift.
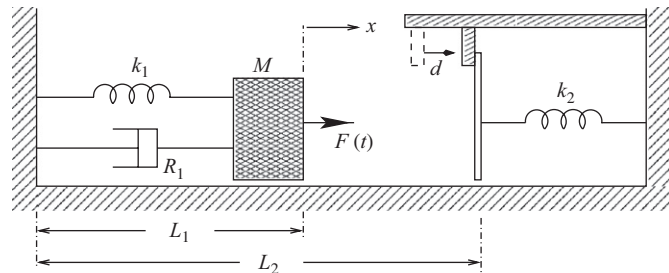
4.3. System C

We now consider the case where the spring k_2 is prestressed by a distance d to the position L_2 as shown in Fig. 10. In this system at the impacting condition (even at zero-velocity) the prestressed spring applies a force on the mass, and so the vector field is non-smooth everywhere on the switching surface. Note that if $d = 0$, it reduces to System-A, and by varying the parameter d, one can introduce various degrees of prestressing. In this system the cushion does not have a dissipative element, which allows us to study the effect of prestressing as distinct from the effect of dissipation.

Subsystem-1 remains unaltered, and Subsystem-2 changes to

$$M\ddot{x} + R_1\dot{x} + (k_1 + k_2)x + (d + L_1 - L_2)k_2 = F\cos\omega t. \tag{43}$$

The results for variation in d (with $R_2 = 0$) are shown in Fig. 11. The most important aspect is that the trace becomes discontinuous

Fig. 10. Schematic diagram of the System-C.

across the grazing condition. Since the value changes over several orders of magnitude and since it has negative value, we plot the logarithm of the negative of the trace. The graph clearly shows that the trace changes discontinuously at the border, and that the value of the trace approaches $-\infty$ as the bifurcation parameter is approached from the right side. In the absence of any dissipation in the cushion, even if there is prestressing in the spring k_2, the determinant remains invariant.

4.4. System D

Now we consider the case where we add a dissipative element to the cushion as shown in Fig. 12. Since all possible parameters are considered, it is now possible to probe the problem of smooth transition from a system with 3/2 singularity to that with square-root singularity. Subsystem-1 remains unaltered, and Subsystem-2 changes to

$$M\ddot{x} + (R_1 + R_2)\dot{x} + (k_1 + k_2)x + (d + L_1 - L_2)k_2$$

$$= F\cos\omega t. \tag{44}$$

The results are given in Figs. 13 and 14.

The determinant is continuous across the grazing condition, and its gradient following grazing depends on the extent of prestressing. On the other hand, the graph of the trace shows that it is continuous only when there is no prestressing, and goes to $-\infty$ if there is
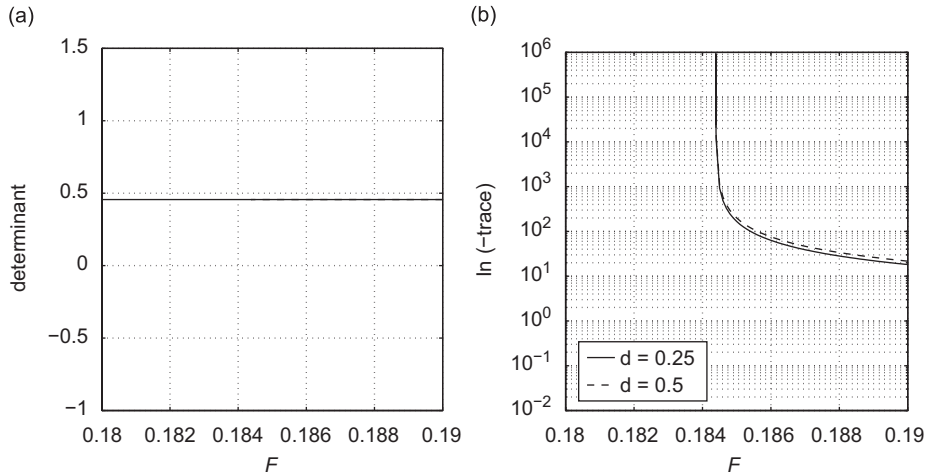
(a)

(b)

Fig. 11. The variation of (a) determinant and (b) trace of the Jacobian matrix of System-C as F is varied through the grazing condition. The parameters are $M = 1$, $k_1 = 1$, $L_2 - L_1 = 0.5$, $\omega = 0.8$, $R_1 = 0.1$. d is varied in steps.
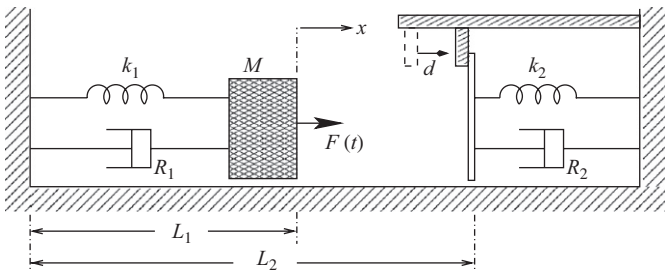

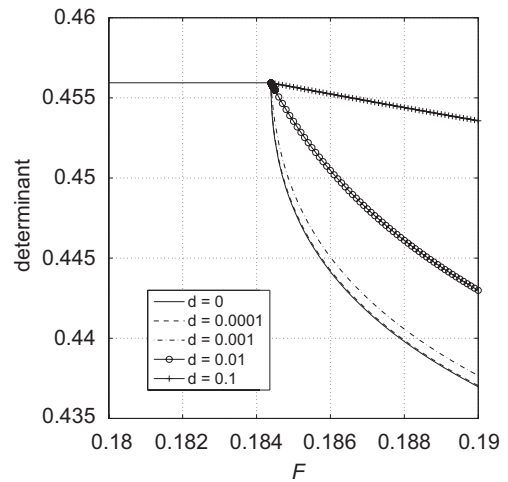**Fig. 12**. Schematic diagram of the System-D.

Fig. 13. The change of determinant of the Jacobian matrix when F crosses the grazing value. The parameters are $m_1 = 1$, $k_1 = 1$, $L_2 - L_1 = 0.5$, $\omega = 0.8$, $R_1 = R_2 = 0.1$.

prestressing. Figs. 14(b) shows how the nature of the curve changes very close to the grazing condition, so that both the square-root singularity and the 3/2 singularity can be exhibited by a single family of functions.

5. Conclusions

In this paper we have systematically studied four system configurations of soft impact oscillator, which has enabled us to reach important conclusions regarding how the Jacobian matrix of the fixed point changes as the system is driven from a non-impacting orbit to an impacting orbit by the change of a parameter. To conduct the numerical investigation, we have adopted a specific technique that allows one to locate the fixed point irrespective of its stability, and to obtain its Jacobian matrix in a single computational procedure. Experiments have been conducted on two system configurations, which validate the results obtained from simulation.

The important conclusions are:

1. For System-A (i.e., where there is no discontinuous change in the vector field), the determinant is invariant, the variation of the trace is continuous, and the derivative of the trace with respect to the parameter tends to infinity as $F \rightarrow F_g^+$, where F_g^+ is the parameter value for the grazing condition.

2. For System-B (i.e., where the vector field changes discontinuously except at the zero-velocity contact point), the determinant varies continuously, and the derivative of the determinant tends to infinity as $F \rightarrow F_g^+$. The change of the determinant following transition to impacting motion depends on the friction of the cushion. The trace behaves in the same way as in System-A.

3. For System-C (i.e., where the vector field changes discontinuously on the switching manifold, but there is no dissipation at the cushion), the determinant remains invariant, the trace varies discontinuously at the grazing condition, and shows a singularity as $F \rightarrow F_g^+$.

4. For System-D (i.e., where all possible system elements are considered), with the smooth variation of prestressing, the curve for the trace changes through a family of functions, from one with 3/2 singularity to one with square-root singularity. The determinant changes continuously following the passage to the
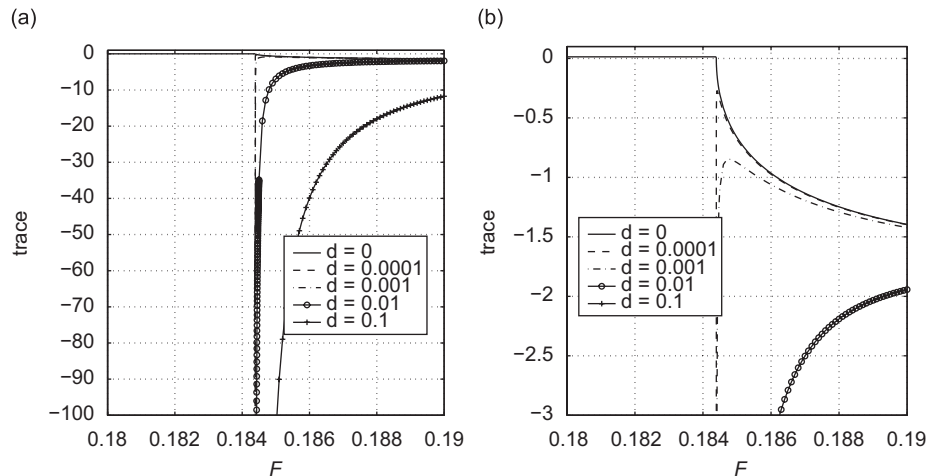
(a)

(b)

Fig. 14. (a) The change of trace for the same condition as in Fig. 13. (b) Enlarged portion showing the family of curves close to the grazing condition.

impacting state, and its derivative at F_g^+ is dependent on the extent of prestressing.

References

[1] A.E. Kobrynskii, Dynamics of Mechanisms with Elastic Connections and Impact Systems, Iliffle Books Limited, London, 1969.
[2] M.I. Feigin, Doubling of the oscillation period with *c*-bifurcations in piecewise continuous systems, Prikl. Mat. Mekh. 34 (1970) 861–869.
[3] A.F. Filippov, Differential equations with discontinuous right-hand side, Am. Math. Soc. Trans. 42 (2) (1978) 199–231.
[4] A.F. Filippov, Differential Equations with Discontinuous Righthand Sides, Kluwer Academic Publishers, Dordrecht, 1988.
[5] S.W. Shaw, P.J. Holmes, A periodically forced piecewise linear oscillator, J. Sound Vib. 90 (1) (1983) 129–155.
[6] A.B. Nordmark, Non-periodic motion caused by grazing incidence in an impact oscillator, J. Sound Vib. 145 (2) (1991) 279–297.
[7] F. Peterka, J. Vacik, Transition to chaotic motion in mechanical systems with impacts, J. Sound Vib. 154 (1) (1992) 95–115.
[8] S. Lenci, G. Rega, A procedure for reducing the chaotic response region in an impact mechanical system, Nonlinear Dyn. 15 (4) (1998) 391–409.
[9] S.J. Hogan, Heteroclinic bifurcations in damped rigid block motion, Proc. R. Soc. London A 439 (1992) 155–162.
[10] B. Blazejczyk-Okolewska, T. Kapitaniak, Co-existing attractors of impact oscillator, Chaos Solitons Fractals 9 (8) (1998) 1439–1443.
[11] C. Budd, F. Dux, Chattering and related behaviour in impacting oscillators, Philos. Trans. R. Soc. 347 (1994) 365–389.
[12] W. Chin, E. Ott, H.E. Nusse, C. Grebogi, Universal behavior of impact oscillators near grazing incidence, Phys. Lett. A 201 (1995) 197–204.
[13] M. Wiercigroch, Dynamics of Discrete Mechanical Systems with Discontinuities (in Polish), TU Silesia University Press, Gliwice, 1994.
[14] M. Wiercigroch, Modelling of dynamical systems with motion dependent discontinuities, Chaos Solitons Fractals 11 (15) (2000) 2429–2442.
[15] D.J. Wagg, G. Karpodinis, S.R. Bishop, An experimental study of the impulse response of a vibro-impacting cantilever beam, J. Sound Vib. 228 (2) (1999) 243–264.
[16] M. Wiercigroch, W.T.V. Sin, Experimental study of based excited symmetrically piecewise linear oscillator, ASME Trans. J. Appl. Mech. 65 (3) (1998) 657–663.
[17] J. Ing, E. Pavlovskaia, M. Wiercigroch, Dynamics of a nearly symmetrical piecewise oscillator close to grazing incidence: modelling and experimental verification, Nonlinear Dyn. 46 (2006) 225–238.
[18] E.K. Ervin, J.A. Wickert, Experiments on a beam-rigid body structure repetitively impacting a rod, Nonlinear Dyn. 50 (3) (2007) 701–716.
[19] H.E. Nusse, E. Ott, J.A. Yorke, Border-collision bifurcations: an explanation for observed bifurcation phenomena, Phys. Rev. E 49 (1994) 1073–1076.
[20] H. Dankowicz, A.B. Nordmark, On the origin and bifurcations of stick-slip oscillations, Physica D 136 (2000) 280–302.
[21] J. Molenaar, J.G. de Weger, W. van de Water, Mappings of grazing-impact oscillators, Nonlinearity 14 (1) (2001) 301–321.
[22] M. di Bernardo, P. Kowalczyk, A.B. Nordmark, Bifurcations of dynamical systems with sliding: derivation of normal-form mappings, Physica D 170 (2002) 175–205.
[23] M. di Bernardo, C.J. Budd, A.R. Champneys, Normal form maps for grazing bifurcations in *n*-dimensional piecewise smooth dynamical systems, Physica D 160 (2001) 222–254.
[24] Y. Ma, M. Agarwal, S. Banerjee, Border collision bifurcations in a soft impact system, Phys. Lett. A 354 (4) (2006) 281–287.
[25] H.E. Nusse, J.A. Yorke, Border-collision bifurcations including "period two to period three" for piecewise smooth maps, Physica D 57 (1992) 39–57.
[26] S. Banerjee, C. Grebogi, Border collision bifurcations in two-dimensional piecewise smooth maps, Phys. Rev. E 59 (4) (1999) 4052–4061.
[27] G.H. Yuan, Shipboard crane control, simulated data generation and border collision bifurcations, Ph.D. Thesis, University of Maryland, College Park, USA, 1997.
[28] W.T.V. Sin, M. Wiercigroch, The design of a symmetrically piecewise oscillator for measurement of chaotic vibration, Proc. Inst. Mech. Eng. Part C 213 (1999) 241–249.
[29] J. Ing, E.E. Pavlovskaia, M. Wiercigroch, S. Banerjee, Experimental study of impact oscillator with one sided elastic constraint, Philos. Trans. R. Soc. A 366 (2008) 679–704.
[30] J.K. Hale, Ordinary Differential Equations, Wiley, New York, 1969.